Appl Phys B (2009) 94: 85–94
DOI 10.1007/s00340-008-3308-8

Applied Physics B
Lasers and Optics

Incoherent broadband cavity enhanced absorption spectroscopy for in situ measurements of NO_2 with a blue light emitting diode

T. Wu · W. Zhao · W. Chen · W. Zhang · X. Gao

Received: 8 April 2008 / Revised version: 27 October 2008 / Published online: 20 November 2008

Abstract We report on the development of Incoherent Broadband Cavity Enhanced Absorption Spectroscopy (IBBCEAS) using a blue light emitting diode (LED) for the detection of NO_2 in laboratory ambient air. Absorption of the oxygen collisional pair in the atmosphere was also detected in the same spectral range. The mirror reflectivity was determined using a standard gas sample mixture of NO_2, and calibrated with the help of the absorption spectrum of the oxygen collisional pair in pure oxygen at atmospheric pressure. Optimization of the experimental parameters was investigated and is discussed in detail. For the first time in IBBCEAS involving broadband absorption spectra, averaging time for signal-to-noise ratio enhancement has been optimized using Allan variance plot. 18.1 ppbv NO_2 in laboratory ambient air has been retrieved from the absorption spectra using differential fitting method over a 40 nm spectral region centered at 470 nm. A minimum detection sensitivity of about 2.2 ppbv (1σ) for NO_2 at atmospheric pressure has been achieved using the optimal averaging time of 100 s by means of a high finesse optical cavity formed with two moderate reflectivity (∼99.55%) mirrors. No purging of the cavity mirrors by high purity He or N_2 gas streams was necessary to prevent contamination of the mirror faces for the in situ measurements.

T. Wu · W. Zhao · W. Zhang · X. Gao (✉)
Anhui Institute of Optics and Fine Mechanics, The Chinese Academic of Sciences, Hefei 230031, China
e-mail: xmgao@aiofm.ac.cn
Fax: +86-551-5591560

W. Chen
Laboratoire de Physicochimie de l'Atmosphère, CNRS UMR 8101, Université du Littoral Côte d'Opale, 189A, Av. Maurice Schumann, 59140 Dunkerque, France

PACS 07.88.+y · 07.60.Rd · 42.60.Da

1 Introduction

Oxides of nitrogen (NO, NO_2) play a central role in atmospheric chemistry, despite their relatively low abundance, in the process of controlling the production of tropospheric ozone, contributing to acid precipitation, and forming other atmospheric oxidants such as the nitrate radical [1]. Nitrogen dioxide (NO_2) is one of the most prevalent air pollutants causing photochemical smog and acid rain. Continuous exposure to even low NO_2 levels can contribute to respiratory health hazard. Typical troposphere NO_2 mixing ratio varies from less than 100 pptv (parts per trillion by volume) in rural areas to several hundreds ppmv (parts per million by volume) in heavily polluted areas.

Many technologies have been developed for the measurements of atmospheric NO_2. Conventional measurement of NO_2 concentrations is carried out based on chemiluminescence [2], laser induced fluorescence (LIF) [3–5], and differential optical absorption spectroscopy (DOAS) [6].

Technology based on high finesse cavity, such as cavity ring down spectroscopy (CRDS) or cavity enhanced absorption spectroscopy (CEAS) [7–11], can provide high sensitivity for detection of absorbing species. Wada et al. [12] demonstrated a continuous-wave diode CRDS system operating at 410 nm for retrieval of NO_2 mixing ratios in ambient air with a detection limit of 0.1 ppbv in 50 s at atmospheric pressure. The spectral range around 410 nm is interference free for NO_2 absorption measurements. Osthoff et al. [13] constructed a pulsed cavity ring-down spectrometer for simultaneous measurements of nitrogen dioxide, nitrate radical (NO_3), and dinitrogen pentocide (N_2O_5) in the atmosphere. The NO_2 detection limit (1σ) for 1 s data was

40 pptv with an uncertainty within ±4% under laboratory conditions. Kasyutich et al. [14] applied phase-sensitive, off-axis cavity-enhanced absorption spectroscopy technique to the measurement of NO_2 in the diluted standard mixture and laboratory air. A noise equivalent detection limit of 1–2 ppbv was achieved with a lock-in amplifier time constant of 1 s. Cavity enhanced absorption spectroscopy system using broadband light sources such as Xe arc lamps and light emitting diodes (LED) has been rapidly developed in recent years. Kebabian et al. [15] demonstrated a NO_2 detector based on cavity-attenuated phase shift spectroscopy using a broadband light emitting diode with a central wavelength of 430 nm. Sensitivity at the shot noise limit of 0.3 ppbv with an integration time of 600 s was reported. Langridge et al. [16] developed a compact cavity enhanced spectrometer based on LED for field detection of atmospheric NO_2 with statistical uncertainty approaching 100 pptv for a 60 s averaging period. The primary advantages of the LED used as light source, compared to Xe arc lamp, are its compact structure, stable radiance, long life time, low power consumption, low cost, and easiness to drive.

In comparison to laser-based CRDS or CEAS, the experimental setup of incoherent broadband cavity enhanced absorption spectroscopy (IBBCEAS) [16–22] is extremely simple, and suitable as robust portable in situ instrument for detection of atmospheric trace gases. By use of an incoherent LED as a light source, the need for mode matching and dithering the optical cavity (for CRDS) or off-axis alignment (for off-axis integrated cavity output spectroscopy, OA-ICOS) can be avoided.

Although the spectral resolution in IBBCEAS is not as high as in laser-based CRDS or CEAS, spectral resolution of <1 nm is usually sufficient for selective recognition of the spectral "fingerprint" of gases in the visible and UV spectral regions. The apparent advantage of IBBCEAS, compared to laser-based CRDS or CEAS techniques, is the capability of handling sophisticatedly the interferences from other absorbers. IBBCEAS can cover a wide spectral range, and multiple absorbers can thus be simultaneously measured. The interference from other absorber can be differentiated by differential fitting method, as employed in DOAS. In CRDS or CEAS experience, dealing with interferences is usually realized by selection of a special wavelength where no interfering constituents exhibit sufficient absorption and by efficient removal of the analyte of interest by chemical scrubber to obtain background spectrum for concentration retrieval. Accuracy of the measured absorber concentration strongly depends on the efficiency of chemical scrubber. The need for improvement in IBBCEAS is the response time. Because of the low spectral radiances of incoherent light source and low efficiency of coupling light into the cavity, the response time generally consume in the minutes time scale.

We report in this paper on the development of incoherent broadband cavity enhanced absorption spectroscopy using LED over a wide spectral range from 450 to 490 nm. This work is motivated by the need for a compact, low-cost, sensitive, and accurate device for measuring trace amounts of NO_2 at the ppbv level for environmental pollution monitoring and understanding the chemical processes in the troposphere. Allan variance study has been carried out, for the first time, to investigate the system's sensitivity as a function of time and the system's stability time. The Allan variance plot shows good system stability of about 100 s, which allows us to determine the optimal averaging time for maximal signal-to-noise ratio (SNR) measurements of NO_2. A minimum detection sensitivity of about 2.2 ppbv (1σ) for NO_2 at atmospheric pressure has been achieved with 100 s exposure time by means of a high finesse optical cavity formed with two moderate reflectivity (∼99.55%) mirrors. No purging of the cavity mirrors by high purity He or N_2 gas streams was necessary to prevent contamination of the mirror faces for the in situ measurements. The measurements of O_2–O_2 absorption in ambient air was performed in the present work, which demonstrated a promising in situ calibration technique by using absorption spectrum of O_2–O_2 in ambient air.

2 Experimental details

2.1 Experimental setup of IBBCEAS

The IBBCEAS experimental setup is depicted in Fig. 1. The selected high power blue LED (LXHL-LR3C, Lumileds Luxeon) has an emission spectrum peaked at 455 nm, as specified by the manufacturer. It requires 3 W of electrical power and provides a radiometric power of 340 mW. The LED was mounted on a cooling plate equipped with a temperature sensor (AD590, Analog Device) for temperature stabilization. A single-stage thermoelectric cooler (TEC) was mounted between the heat sink and the cooling plate. The temperature controller (MPT-10000, Wavelength Electronics) used the feedback signal from the sensor to adjust the current flow through the TEC to maintain the LED at the desired temperature and provided long-term temperature stability with $\delta T \leq 0.1$°C, which was necessary to reduce the effects of temperature fluctuation on the detection limit [23]. The LED was fed with a current of 0.8 A whose stability was better than 0.1%. The light emitted from the LED was directly coupled into a multimode optical fiber (1000 μm in diameter with a numerical aperture of NA = 0.22). The LED light leaving the fiber was focused, via a focusing lens ($f = 100$ mm), into an optical cavity formed with two high reflectivity mirrors. In order to reduce stray light and define the light beam diameter on the input mirror of the cavity, an iris was set in front

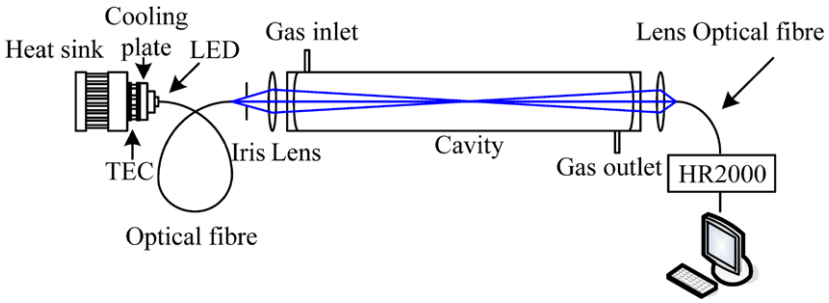

Fig. 1 Experimental set-up for incoherent broadband cavity enhanced absorption spectroscopy using a blue LED. TEC: thermoelectric cooler; HR2000: high-resolution miniature fiber optic spectrometer

of this focusing lens that was placed close to the front cavity mirror. The cavity mirrors (1 m radius of curvature and 30 mm in diameter) had a maximum reflectivity of 99.7% around 480 nm, as specified by the manufacturer, and were separated by a distance of 97.5 cm. The active sampling region was 92.5 cm long and enclosed with PTFE tubing. The light transmitted through the cavity was focused, with a collecting lens ($f = 50$ mm) placed closely behind the rear cavity mirror, into a multimode optical fiber (1000 µm diameter and 0.22 numerical aperture). The fiber was connected to a high-resolution spectrometer (HR2000, Ocean Optics) in a Czerny–Turner configuration. The spectrograph was equipped with a 50 µm entrance slit, a 600 grooves/mm holographic grating and a 2048 pixels linear CCD array with a 12-bit A/D vertical resolution (Sony ILX511), which allowed covering the whole 350–800 nm spectral range with a typical resolution of 0.9 nm (full width at half maximum, FWHM). This spectral resolution is sufficient for selective recognition of the spectral absorption structure, since NO_2 has a well developed spectral structure in the UV and visible region even at around 1 nm resolution [22]. The spectral data was then transferred through a universal serial bus to a PC for data treatment using commercial software (Ocean Optics, OOIBase32).

2.2 Optimization of experimental parameters

2.2.1 Light beam coupling issues

Radiation from the LED to optical fiber Efficiency of coupling light emitted from LED into an optical fiber is affected mostly by the geometrical losses (caused by the cross-sectional area of the optical fiber smaller than the LED radiating area imaged on the fiber) and the angular losses resulting from the mismatching between the LED radiation angle and the fiber numerical aperture. The chip size of the used LED is approximately 1 mm × 1 mm with a radiation divergence of 140° (FWHM) formed by a moulded plastic lens in the front of the LED emitters. In order to reduce the coupling losses resulted from the radiation divergence, the molded plastic was cut away and the remaining surface above the LED was polished to obtain a plane smooth surface so that the LED radiation became quasi-collimated. Maximum coupling efficiency of the LED radiation into the optical fiber was obtained by placing the fiber end as close as possible to the LED emitters. It is desirable to use larger diameter and bigger numerical aperture of optical fiber for efficient collection of the LED radiation.

LED emission from the optical fiber to optical cavity The LED light leaving the optical fiber was focused at the center of a high finesse optical cavity via a focusing lens of $f = 100$ mm. In order to efficiently couple the light into the cavity, we used near-confocal cavity arrangement to reduce the "spillover" losses [15]. In fact, besides diffraction losses which would be reduced by use of larger cavity mirrors, most losses of light in the cavity are attributed to "spillover" losses, due to the fact that light departs far from the cavity axis and reaches the wall of the cavity or the rims of the cavity mirrors before the light is transmitted through the cavity. The near-confocal cavity arrangement may considerably reduce the "spillover" losses, if the beam diameter is less than the effective aperture of the cavity. In the present work, the effective cavity aperture is about 22 mm in diameter.

LED light leaked from the cavity to an optical fiber connected to the spectrometer LED light leaked out from the cavity was focused into a multimode optical fiber connected to the spectrometer. In order to optimize the coupling efficiency, appreciate f-number ($f\#$) should be chosen. The f-number is the ratio of the focal length (f) of the lens to its "effective" aperture (D) that corresponds to the effective aperture of the cavity in our experimental configuration. The f-number defines the angle of the cone of light leaving the lens which ultimately forms the image on the optical fiber. The maximum light coupling would be realized when the angle (θ_{light}) of the focusing light cone is less than the value of θ_{fiber} determined by the numerical aperture (NA_{fiber}) of the optical fiber, where θ is the angle made by the marginal ray with the optical axis. The numerical aperture NA is defined as

$$\text{NA} = n \sin\theta, \tag{1}$$

where n is the index of refraction of the medium in which the light beam propagates. It is thus easy to obtain the fol-

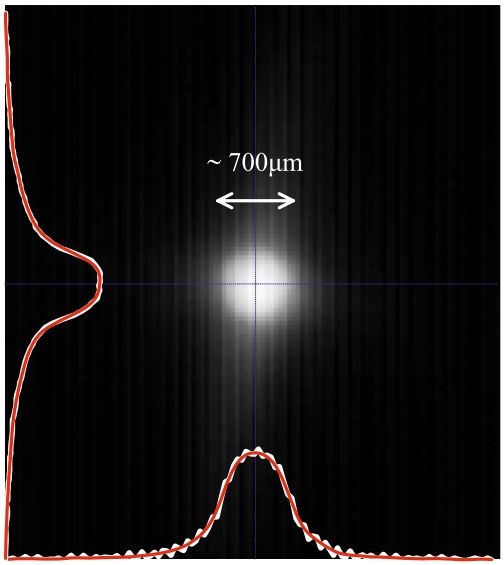

Fig. 2 Light pattern leaked out the rear cavity mirror imaged with a CCD. It was recorded with a light beam of 6 mm diameter on the front cavity mirror. The central pattern is about 700 μm in diameter. *White lines*: the intensity profile; *red lines*: filtered profile

lowing condition that should be realized for an optimal light coupling:

$$f\# = \frac{f}{D} \geq \frac{1}{2 \times \mathrm{NA}_{\mathrm{fiber}}}. \tag{2}$$

In our experience, a focal length of $f = 50$ mm has been chosen for an effective cavity aperture of $D = 22$ mm, leading to an $f\#$ of 2.27 that satisfied (2) with a $\mathrm{NA}_{\mathrm{fiber}}$ of 0.22.

2.2.2 *Optical cavity alignment issue*

A focused light injection design is less sensitive to alignment drift compared to parallel light injection [24]. The radiation pattern transmitted through the cavity has been studied with the help of a monochrome charged coupled device (CCD) camera to aid in optimizing optical cavity alignment and coupling of cavity output into the optical fiber connected to the HR2000 spectrometer. The CCD was placed at the image plane of the light beam behind the rear cavity mirror. The light beam intensity leaked out from the cavity was directly focused onto the CCD camera and recorded. Optimal cavity alignment would be obtained with perfectly overlapping of the spots resulted from two cavity mirrors, which would result in a symmetrical intensity distribution for maximum output of the LED light leaked out from the cavity. The image of the light pattern leaked out of the rear cavity mirror, shown in Fig. 2, was observed for the maximum optical output intensity. The central pattern of the imaged light beam on the CCD is about 700 μm in diameter with a light beam of 6 mm diameter on the front cavity mirror. It is natural to assume that, by increasing the diameter of the incident beam on the input mirror of the cavity (which can be achieved by enlarging the aperture of the iris placed in front of the focusing lens), we will be able to inject more lights into the cavity and collect more light leaked out of the cavity by use of a fiber with larger diameter. A practical compromise, between higher light intensities (by using larger incident beam diameter) and the availability of the optical fiber diameter, yielded the actual choice used in our experiment: 6 mm diameter beam was coupled to the cavity and the transmitted beam was focused to a spot of 700 μm diameter on a multimode optical fiber of 1 mm diameter.

2.2.3 *Stability of the spectral source emission*

Stability of the LED emission spectrum extraordinarily depends on the stabilities of the temperature [23] and the current provided by the power supply. The emission wavelength is dominated by the bandgap energy of semiconductor materials. The bandgap energy of all semiconductor materials is a function of temperature. Apart from the emission wavelength, periodic narrowband spectral structures (see Fig. 4) are also susceptible to temperature change. These oscillation-like structures are attributed to Fabry–Perot etalon effect that occurs inside the LED structure. The etalon structure is temperature dependent, so the peak wavelengths of the etalon will shift when temperature changes. For our experimental setup, we observed that the absorption signal was completely submerged by etalon noise when the temperature stability of the cooling plate was >1°C, and no evident etalon noise could be observed when temperature stability of the cooling plate was <0.1°C. A temperature controller MPT-10000 with long term stability of <0.008°C was used in our work to provide a long-term temperature stability of ≤ 0.1°C. For field application, it may be a problem when temperature-controlled system of the LED is disturbed by ambient temperature change. In this case, background measurements and corrections should be regularly repeated and the slowly varying temperature-dependent etalon structure can be removed by using synthetic etalon references, as described in [23]. The stability of current supply in our present work was better than 0.1%.

Because of low spectral radiances of the incoherent light source and low light coupling efficiency, long integration time for CCD detector is usually used to improve the detection sensitivity. However, it may result in CCD saturation at the edges of high reflectivity range of the cavity mirrors when the integration time is too long. As a compromise, integration time of 25 ms was used in our experiments.

2.2.4 *Allan variance study*

Allan variance can be used to study the important performance characteristics, such as stability and sensitivity of spectroscopy-based analytical instruments [25, 26]. Allan

variance calculation is usually carried out on a recorded set of N time-series data referring to amplitude. For IBBCEAS involving broadband absorption spectra, Allan variance study at a single frequency (a single CCD pixel) cannot describe the system performance over the full spectral range. In the present work, Allan variance has been calculated for each CCD pixel within the spectral range of 450–490 nm, and then the averaged Allan variance has been plotted for estimating the entire system's stability and sensitivity, which permits one to determine the optimal averaging time for maximal SNR. For this purpose, the light intensity from the cavity was monitored over 200 consecutive 2.5 s spectra (i.e., 100 averaged spectra with 25 ms integration time), when the cavity was flushed by pure nitrogen at a flow rate of 600 sccm. The N elements of the recorded light intensity values $Y_{p,n}$ were divided into M groups containing K data points (p is the CCD pixel, $p = 1, 2, \ldots, P$, $P = 178$ within the range 450–490 nm, and $n = 1, 2, \ldots, N$, $N = 200$), and then averaged within these groups [14, 27]:

$$X_{p,i}(K) = \frac{1}{K}\sum_{m=1}^{K} Y_{p,ik+m}, \quad i = 0, 1, 2, \ldots, M;$$
$$M = N/K - 1. \tag{3}$$

The Allan variance of these M averaging values $X_{p,i}$ for each CCD pixel p within the range of 450–490 nm was then calculated using the following expression:

$$\sigma_A^2(p, K) = \frac{1}{2M}\sum_{i=1}^{M}\left(X_{p,i+1}(K) - X_{p,i}(K)\right)^2, \tag{4}$$

and the averaged Allan variance can be determined by:

$$\overline{\sigma_A^2(K)} = \frac{1}{P}\sum_{p=1}^{P}\sigma_A^2(p, K). \tag{5}$$

The averaged Allan variance was plotted as a function of the averaging time, $\tau = K \times t_0$ ($t_0 = 2.5$ s) in Fig. 3. As can be seen, the stability time of the system was 100 s, so the optimum averaging time for SNR enhancement was limited to be 100 s, which corresponds to an optimum averaging number of 4000.

3 Result and discussions

3.1 Determination of cavity mirror reflectivity

Cavity enhanced absorption spectroscopy is based on measuring the intensity of light transmitted through a high finesse optical cavity as a function of wavelength. The cavity output intensity can be written as [17]:

$$I = I_{\text{in}}\frac{T^2(1-L)}{1-R^2(1-L)^2}, \tag{6}$$

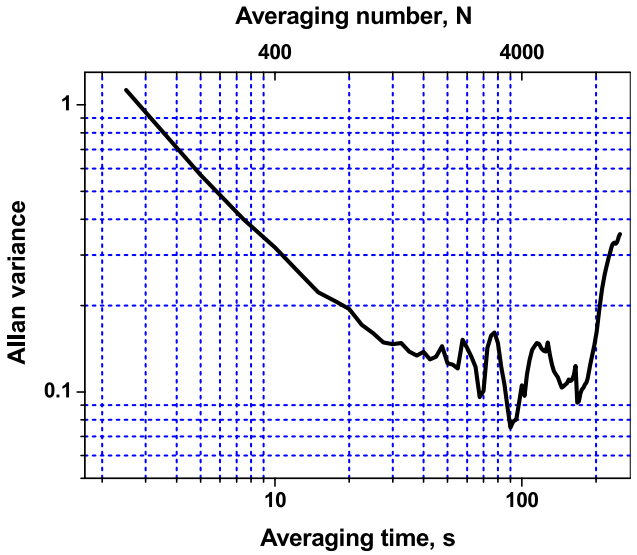

Fig. 3 Allan variance plot as a function of averaging time. Optimum averaging time is about 100 s, corresponding to an optimum averaging number of 4000

where R is the mirror reflectivity, T is the corresponding transmittance, and I_{in} is the light intensity injected into the optical cavity. L in (6) describes all optical losses including absorption loss of interest L_a, time independent "background losses" L_b resulted from molecular scattering (Rayleigh) and particulate-matter scattering (Mie) in the cavity. The overall loss L is then given by the following expression [18]:

$$L = 1 - (1 - L_a)(1 - L_b). \tag{7}$$

In our work, Rayleigh scattering was accounted for by recording background spectra with cavity purged with pure nitrogen. Atmosphere aerosol was removed by a Teflon filter connected to the cavity inlet. Assuming the losses per pass to be solely due to Lambert–Beer absorption, i.e.,

$$1 - L = \exp(-\alpha d), \tag{8}$$

where d is the effective cavity length of the region containing the absorber, and $\alpha = N\sigma$ is the total extinction (where N is the number of absorbing molecules per cubic centimeter and σ is the cross-section of the absorber of interest). For cavity-based absorption spectroscopy, the total extinction α can be described as follows [14]:

$$\alpha = -\frac{1}{d}\ln\left[\frac{1}{2R^2}\left[\frac{I_0((\text{Re}^{-\alpha_{\text{Ray}}d})^2 - 1)}{Ie^{-\alpha_{\text{Ray}}d}} + \sqrt{\left(\frac{I_0(1 - (\text{Re}^{-\alpha_{\text{Ray}}d})^2)}{Ie^{-\alpha_{\text{Ray}}d}}\right)^2 + 4R^2}\right]\right], \tag{9}$$

where α_{Ray} is Rayleigh scattering coefficient of the purge gas (N_2 at 1 atm), and I_0 is the corresponding time integrated transmitted intensity. For small losses per pass ($L \to 0$), high mirror reflectivity ($R \to 1$) and $e^{-\alpha_{\mathrm{Ray}} d} \to 1$, the extinction coefficient α can be approximated by:

$$\alpha = \frac{1}{d}\left(\frac{I_0}{I} - 1\right)(1 - R). \tag{10}$$

Absorber concentration can thus be retrieved using differential fitting method based upon (10). This method, usually used in differential optical absorption spectroscopy, is capable of accounting for slow variation in LED emission intensity.

For quantitative analysis application, the mirror reflectivity over the spectral region of interest needs to be accurately determined. In cavity ringdown absorption spectroscopy, the mirror reflectivity is derived by the measurement of empty cavity decay time. In CEAS, the mirror reflectivity is usually determined based on the measurement of species absorption with known concentration. In the present work, standard NO_2 mixture was used for mirror reflectivity measurement. The accuracy of the measurements strongly depends upon the uncertainty in NO_2 absorption cross-section and the actual NO_2 concentration in the cell. As NO_2 is well known to be a very "sticky" molecule, the adsorption effects resulting in NO_2 concentration loss should be thoroughly considered. In our experience, even though PTFE tubing was used and the measurements were performed under flow condition in order to reduce wall adsorption, NO_2 loss may still be a result from adsorption in NO_2 mixture cylinder, in stainless-steel pressure regulator and in gas connection lines. In this context, the cavity mirror reflectivity determined over the spectral region of 450–490 nm based on the absorption spectrum measurement of the standard NO_2 mixture was considered as relative reflectivity. We then measured absorption of the oxygen collisional pair resulting from the weak ${}^1\Sigma_g^+ + {}^1\Delta_g \leftarrow {}^3\Sigma_g^- + {}^3\Sigma_g^-$ transition in the region of 460–490 nm for absolute calibration of the measured relative mirror reflectivity. This method was also recently reported by Langridge et al. [28].

As the overall performance of the setup as a function of time may affect the measurements of $(1 - R)$ as well as I_0, the measurements of the cavity mirror's reflectivity have been carried out within the system's stability time. In our experience, a flow (600 sccm) of the standard NO_2 mixture (860 ppbv NO_2 in N_2) and pure N_2 was subsequently injected into the cavity (at 1 atm). Figure 4 shows the cavity output spectra of the standard NO_2 mixture (I) and pure N_2(I_0), respectively, which have been recorded with a 25 s exposure time (integration time: 25 ms, spectra averaged: 1000). The absorption cross-section of NO_2 was generated by convoluting the high-resolution cross-section spectrum reported by Burrows et al. [29] with an instrument function of 0.9 nm (FWHM) of the spectrometer used in the present work. With the known absorption cross-section and known NO_2 concentration in the cavity, the absorption coefficient has been determined, and then the mirror reflectivity as a function of wavelength in the 450–490 nm range was deduced based on (10).

The measurement of O_2–O_2 absorption in pure oxygen performed under atmospheric pressure is shown in Fig. 5. The spectrum was recorded with a 100 s exposure time (integration time: 25 ms, spectra averaged: 4000) for I_0 and I, respectively. Absorption cross-section of the oxygen collisional pair reported by Greenblatt et al. [30] was used. The fit to the absorption coefficient of oxygen collisional pair is shown in Fig. 5. The volume mixing ratio of the oxygen collisional pair to oxygen derived from the fit is 1.02 ± 0.01. Minimal absorption coefficient of 1.23×10^{-8} cm^{-1} was deduced from the standard deviation of the residuals between the measured and the fitted absorption coefficient.

The calibrated mirror reflectivity over 450–490 nm is given in Fig. 4 (blue curve in the top panel). Maximum reflectivity of 0.9955 was found with an uncertainty of 0.0001 over the range 481–483 nm. Considering the uncertainties in the cross-section of O_2–O_2(2%), in the O_2 pressure within the cavity (1%), in the cavity length (1%), and in $\Delta I/I$ (0.1%), the estimated uncertainty in the factor $(1 - R)$ is approximately 4.6%.

3.2 Measurements of NO_2 in laboratory ambient air

To evaluate the instrumental performance, in situ measurements of NO_2 in laboratory ambient air was performed at a temperature of 284 K and a pressure of 760 torr on the night of February 28, 2008. A parking lot is located close to the laboratory. The windows of the laboratory were opened during the measurements.

3.2.1 Measurement protocol

Background measurement (in the absence of absorber of interest) is very important for accurately retrieving the concentration of the absorber, as well as for checking the cleanliness of the cavity mirrors and optical alignment of the cavity. Several methods for background measurement have been reported in the literature [13, 14, 31]. Zero air or chemical scrubber is usually used to acquire "true" background spectrum for retrieval of ambient NO_2 mixing ratio. The universally employed method in CRDS-based experience is to use a chemical scrubber, such as hydroxyapatite ($Ca_{10}(PO_4)_6(OH)_2$), on a TiO_2 substrate, which allows recording a "true" background spectrum by eliminating NO_2 in the air sample. However, any other interfering species absorbing in the same wavelength range, which may be removed by the chemical scrubber, could contribute in overestimating the NO_2 concentration. In addition, the chemical scrubber has a short utilization lifetime. In the present

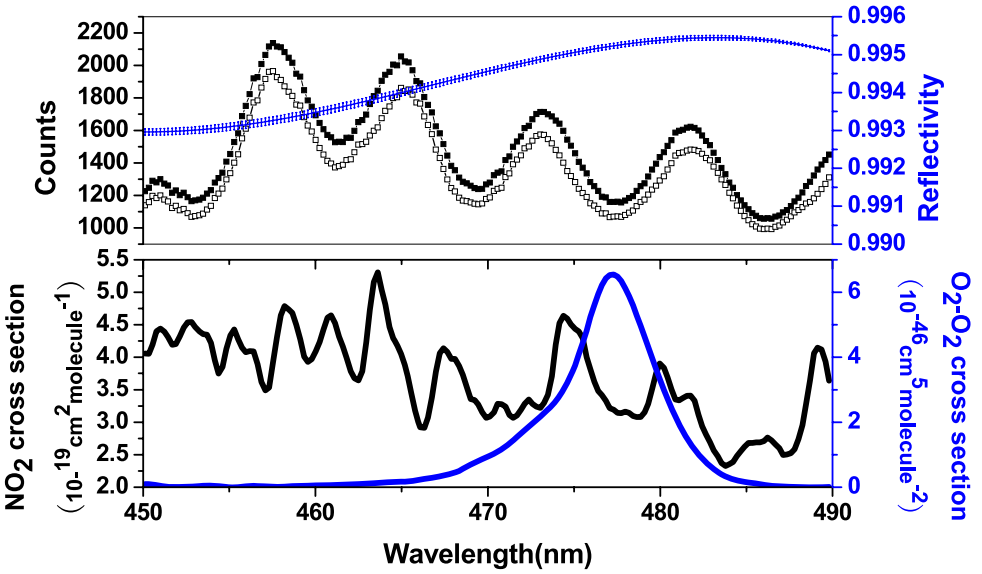

Fig. 4 *Top panel*: cavity output spectra for standard NO_2 mixture (*open circle*) and pure N_2 (*solid circle*). The deduced mirror reflectivity against wavelength is also shown in the same spectral region (*blue line* with *error bars*). *Bottom panel*: absorption cross-section of NO_2 and O_2–O_2 used in the present work

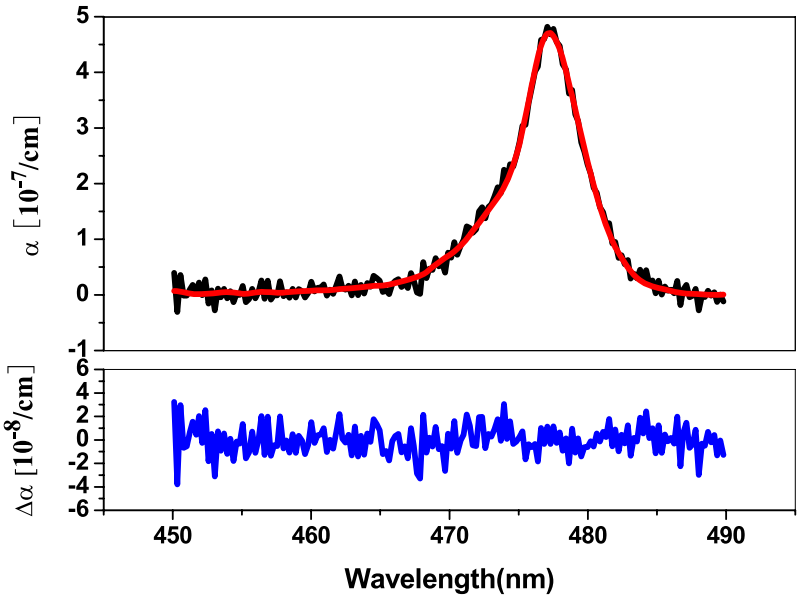

Fig. 5 The *top panel* shows absorption coefficient of oxygen collisional pair in the pure oxygen. The volume mixing ratio of oxygen collisional pair to oxygen is 1.02 ± 0.01. The *bottom panel* shows residual spectrum with standard deviation of 1.23×10^{-8} cm^{-1}

work, background was determined by flushing the cavity with a pure N_2 flow and then recording the baseline spectrum over the same spectral range. This method is, however, not convenient for CRDS, since the analyte concentration derived from the pure N_2 flow-based background spectrum may be overestimated if other absorbers are present in ambient air in the same wavelength range. While in IBBCEAS, all absorbers with narrow absorption feature can be simultaneously detected and retrieved by using differential fitting method. Air sample was pulled through the cavity by a diaphragm pump. The pressure inside the cavity was monitored using a pressure gauge. Measurements were conducted with 100 s exposure time (integration time: 25 ms, spectra averaged: 4000) at a flow rate of 600 sccm for pure N_2 and air sample. In order to minimize the losses of NO_2 in the Teflon filter, we flushed the cavity with ambient air several minutes before measuring.

3.2.2 *Species detectable within the sensor sensitivity in the same spectral range*

In the wavelength range used for the NO_2 measurement, there is also absorption by ozone (O_3), NO_3, water vapor and O_2–O_2, as well as optical power losses resulting from scattering by aerosol. A Teflon filter (pore size: 1 μm) was used to prevent aerosols from entering the cavity and contaminating the cavity mirrors. Regarding O_3 absorption, the maximal absorption cross-section is 8.79×10^{-22} cm^2 molecule^{-1} at 483 nm [32], which only yields a peak absorption of 8.96×10^{-10} cm^{-1} for typical 40 ppbv

O_3 in the atmosphere. With respect to O_3, absorption cross-section of NO_3 in this region is very strong ($\sim 1.06 \times 10^{-18}$ cm^2 molecule^{-1} at 489.8 nm [33]). It is well known that formation of NO_3 is expected at night with high ozone and NO_2 concentration. However, the tropospheric NO_3 concentration at nighttime is relatively low; it varies from 0 to 10 pptv in clean marine environments to several hundred pptv in polluted urban air. This relatively low concentration makes NO_3 absorption (less than 10^{-8} cm^{-1}) ignorable. Regarding water vapor whose high resolution structure is degraded by the low resolution of the used spectrometer [34], the maximal absorption is about 1.5×10^{-9} cm^{-1} at 472 nm for a water vapor mixing ratio of 0.6% in laboratory ambient air (48% relative humidity at 284 K). Owing to the squared dependence of the O_2–O_2 concentration on oxygen ($\sim$21% for O_2 in the atmosphere), absorption of O_2–O_2 in air is approximately 1.78×10^{-8} cm^{-1} at the peak wavelength of 477 nm.

Based on the minimum detectable absorption coefficient of the developed instrument ($\sim 1.23 \times 10^{-8}$ cm^{-1}) in comparison with the absorption intensities mentioned above for the molecules present in the spectral region of 450–490 nm, the mostly detectable absorber other than target molecule is O_2–O_2.

3.2.3 *Concentration retrieval*

From the measurements of NO_2 and O_2 absorption spectra, their concentrations were deduced using least-squares fit of differential cross-section to the measured differential absorption coefficient, according to (11) [35]:

$$\Delta\alpha(\lambda) = n_{NO_2}\Delta\sigma_{NO_2}(\lambda) + n_{O_2-O_2}\Delta\sigma_{O_2-O_2}(\lambda), \tag{11}$$

where n_{NO_2} and $n_{O_2-O_2}$ are the number densities [molecule cm^{-3}] of NO_2 and O_2–O_2, $\Delta\sigma_{NO_2}(\lambda)$ and $\Delta\sigma_{O_2-O_2}(\lambda)$ are the corresponding differential cross-sections [cm^2 molecule^{-1}], respectively. $\Delta\alpha(\lambda)$ is the differential absorption coefficient [cm^{-1}]. The NO_2 cross-section $\sigma_{NO_2}(\lambda)$ and the O_2–O_2 cross-section $\sigma_{O_2-O_2}(\lambda)$ were fitted by polynomials $P_{NO_2}(\lambda)$ and $P_{O_2-O_2}(\lambda)$, respectively. Then the differential cross-sections $\Delta\sigma_{NO_2}(\lambda)$ and $\Delta\sigma_{O_2-O_2}(\lambda)$ were obtained using (12):

$$\begin{aligned}\Delta\sigma_{NO_2}(\lambda) &= \sigma_{NO_2}(\lambda) - P_{NO_2}(\lambda),\\ \Delta\sigma_{O_2-O_2}(\lambda) &= \sigma_{O_2-O_2}(\lambda) - P_{O_2-O_2}(\lambda).\end{aligned} \tag{12}$$

The differential absorption coefficient $\Delta\alpha(\lambda)$ was determined using the same procedure by fitting a polynomial to the measured absorption coefficient and then subsequent subtraction from it. Figure 6 shows the narrow absorption features of NO_2 and the oxygen collisional pair, as well as the residual spectrum resulted from fitting the differential cross-section to the differential absorption coefficient. The corresponding ambient NO_2 and oxygen mixing ratios are found to be: 18.1 ± 0.8 ppbv and 0.18 ± 0.03. It should be noted that, as the concentrations are retrieved by a numerical analysis of the absorption spectra, the statistical uncertainty in concentrations (4.4% for NO_2 and 16.7% for O_2) from the fit only describes the 1σ statistical errors associated to the spectral fit. They do not include the systematic uncertainty associated to the uncertainties in the cross-sections of NO_2 ($\sim$5%) and O_2–O_2 ($\sim$2%), in the factor $(1 - R)$ ($\sim$4.6%), in $\Delta I/I$ (0.1%), and in the cavity length (1%). For NO_2, the total measurement uncertainty of concentration combined with the statistical uncertainty from the fit is approximately estimated to be within 10%. For oxygen, the total uncertainty of concentration is dominated by larger statistical uncertainty from the fit, which is attributed to lower SNR of the measured O_2–O_2 absorption spectrum. The standard deviation of the residuals between the measured and the fitted absorption coefficients is 1.26×10^{-8} cm^{-1}(for an exposure time of 100 s), which corresponds to 1σ minimum detectable absorption coefficient (SNR = 1). The increased noise at the short wavelength observed in Fig. 6 may be caused by the decrease of the cavity mirror reflectivity at the spectral edges.

As the windows of the laboratory were opened during the measurements, the relatively high NO_2 concentration in laboratory air may be partly attributed to the activity on the parking lot. As the experiments were performed under flow condition, the inlet losses can be minimized.

In cavity enhanced absorption spectroscopy-based trace gas detection scheme, ultra-high reflectivity cavity mirrors may be subject to performance degradation by dust or pollutants deposition on the mirrors, which will affect the detection sensitivity and the concentration determination. In this case, cavity mirrors are usually protected from impinging contaminants by using high purity N_2 or He gas streams to purge the regions near mirrors. In our experiment, considering the moderate mirror reflectivity that was not as vulnerable to environmental pollution as high reflectivity mirror, the mirrors were not purged. Two spectra of pure N_2 were acquired before and after the measurements of laboratory air in order to verify the mirror reflectivity. No degradation of mirror performance was observed after usage and exposure to laboratory air over a period of several days.

Based on the SNR of 8 for the experimental NO_2 differential absorption spectrum, estimated by the ratio of the maximal absorption difference to the standard deviation of the residuals, 1σ detection limit of 2.2 ppbv was deduced for the present experimental instrument. The detection sensitivity can be further improved by using cavity mirrors with higher reflectivity. Higher detection limit of 0.1 ppbv (for a 60 s average period) has been reported by using higher reflectivity mirrors ($R > 99.976\%$) [16]. Longer cavity, as

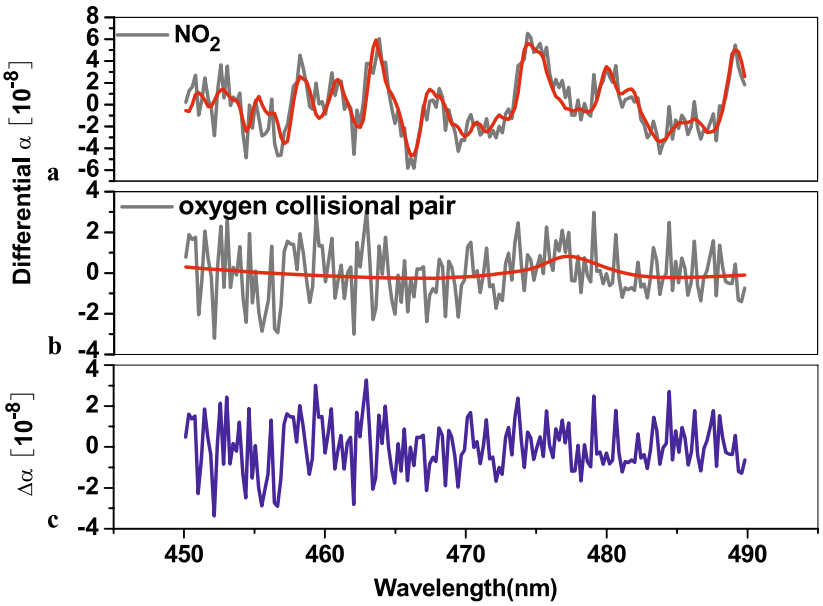

Fig. 6 Experimental (*grey*) and fitted (*red*) differential absorption spectra of NO_2 (**a**) and the oxygen collisional pair (**b**) in laboratory ambient air. The concentrations deduced from the fit are 18.1 ± 0.8 ppbv for NO_2 and 0.18 ± 0.03 for oxygen mixing ratio with an acquisition time of 100 s. **c** Residual spectrum with a standard deviation of 1.26×10^{-8} cm^{-1}

alternative approach, can be used to improve detection sensitivity. The authors of [19] reported NO_3 detection with a measured sensitivity of 4 pptv in a 4.5 m long cavity. In addition, cooling CCD array of the spectrometer may also reduce the detector noise.

4 Conclusions

Development of a compact, low-cost, sensitive, and accurate instrument for quantifying trace amounts of NO_2 in ambient air is achieved by using LED-based incoherent broadband cavity enhanced absorption spectroscopy over the region of 450–490 nm. For the first time, averaged Allan variance has been studied for an IBBCEAS-based spectroscopic instrument over the full spectral range of 450–490 nm. The Allan variance plot was used to evaluate the system performance and to determine the optimal averaging time for SNR enhancement. 18.1 ppbv NO_2 in laboratory air was measured with a detection limit of about 2.2 ppbv using an optimal averaging time of 100 s.

In MAX-DOAS (multi-axis differential optical absorption spectroscopy) measurements of atmospheric trace gases and aerosol distributions [36–38], absorption by O_2–O_2 is usually used to determine the optical absorption path length. A well-known advantage of this calibration approach is based on the fact of the squared dependence of the O_2–O_2 concentration on oxygen, while the atmospheric column of oxygen varies only slightly depending on pressure and temperature. In our IBBCEAS experience, absorption of O_2–O_2 in pure O_2 was measured and used for absolute calibration of the cavity mirror reflectivity that was initially deduced from the measurement of a standard NO_2 mixture absorption spectrum. Measurements of O_2–O_2 absorption in ambient air were performed in the present work which demonstrated a promising in situ calibration technique by using the absorption spectrum of O_2–O_2 in ambient air. Indeed, the detection sensitivity achieved in the present work should be further improved by use of higher reflectivity mirrors.

Low-cost mirrors with moderate reflectivity (∼99.55%) have been successfully used with sufficient detection sensitivity for NO_2 detection in air. The use of moderate reflectivity mirrors exhibits the following advantage (apart from its low-cost): The mirror performance seems not to be as vulnerable to environmental pollution as high reflectivity mirror. No purging of the cavity mirrors by clean air or N_2 was necessary to prevent contamination of their faces. Under operating conditions, the mirrors remained sufficiently clean for measurements over a period of several days.

Acknowledgements This research was funded by the National 863 High Technology Research and Development Program of China under Grant No. 2006AA06Z237, and in part by the French International Program of Scientific Cooperation (CNRS/PICS No. 3359).

References

1. R.P. Wayne, *Chemistry of Atmospheres* (Oxford University Press, Oxford, 2000)
2. T.B. Ryerson, E.J. Williams, F.C. Fehsenfeld, J. Geophys. Res. **105**, 26447 (2000)
3. J.A. Thornton, P.J. Wooldridge, R.C. Cohen, Anal. Chem. **72**, 528 (2000)
4. J. Matsumoto, J. Hirokawa, H. Akimoto, Y. Kajii, Atmos. Environ. **35**, 2803 (2001)
5. Y. Matsumi, S. Murakami, M. Kono, K. Takahashi, M. Koike, Y. Kondo, Anal. Chem. **73**, 5485 (2001)

6. J.W. Harder, E.J. Williams, K. Baumann, F.C. Fehsenfeld, J. Geophys. Res. **102**, 6227 (1997)
7. A. O'Keefe, D.A.G. Deacon, Rev. Sci. Instrum. **59**, 2544 (1988)
8. R. Engeln, G. Berden, R. Peeters, G. Meijer, Rev. Sci. Instrum. **69**, 3763 (1998)
9. A. O'Keefe, Chem. Phys. Lett. **293**, 331 (1998)
10. J.B. Paul, L. Lapson, J.G. Anderson, Appl. Opt. **40**, 4904 (2001)
11. D.S. Baer, J.B. Paul, M. Gupta, A. O'Keefe, Appl. Phys. B **75**, 261 (2002)
12. R. Wada, A.J. Orr-Ewing, Analyst **12**, 1595 (2005)
13. H.D. Osthoff, S.S. Brown, T.B. Ryerson, T.J. Fortin, B.M. Lerner, E.J. Williams, A. Pettersson, T. Baynard, W.P. Dubé, S.J. Ciciora, A.R. Ravishankara, J. Geophys. Res. D **111**, 12305 (2006)
14. V.L. Kasyutich, P.A. Martin, R.J. Holdsworth, Meas. Sci. Technol. **17**, 923 (2006)
15. P.L. Kebabian, S.C. Herndon, A. Freedman, Anal. Chem. **77**, 724 (2005)
16. J.M. Langridge, S.M. Ball, R.L. Jones, Analyst **131**, 916 (2006)
17. S.E. Fiedler, A. Hese, A.A. Ruth, Chem. Phys. Lett. **371**, 284 (2003)
18. S.E. Fiedler, A. Hese, Rev. Sci. Instrum. **76**, 023107 (2005)
19. D.S. Venables, T. Gherman, J. Orphal, J.C. Wenger, A.A. Ruth, Environ. Sci. Technol. **40**, 6758 (2006)
20. S.M. Ball, J.M. Langridge, R.L. Jones, Chem. Phys. Lett. **398**, 68 (2004)
21. T. Gherman, D.S. Venables, S. Vaughan, J. Orphal, A.A. Ruth, Environ. Sci. Technol. **42**, 890 (2008)
22. M. Triki, P. Cermak, G. Méjean, D. Romanini, Appl. Phys. B **91**, 195 (2008)
23. C. Kern, S. Trick, B. Rippel, U. Platt, Appl. Opt. **45**, 2077 (2006)
24. S.E. Fiedler, A. Hese, U. Heitmann, Rev. Sci. Instrum. **78**, 073104 (2007)
25. P. Werle, R. Mucke, F. Slemr, Appl. Phys. B **57**, 131 (1993)
26. P. Weibring, D. Richter, A. Fried, J.G. Walega, C. Dyroff, Appl. Phys. B **85**, 207 (2006)
27. T. Berg, S. Cherednichenko, V. Drakinskiy, P. Khosropanah, H. Merkel, E. Kollberg, J.W. Kooi, Proc. SPIE **5498**, 605 (2004)
28. J.M. Langridge, T. Laurila, R.S. Watt, R.L. Jones, C.F. Kaminski, J. Hult, Opt. Express **16**, 10178 (2008)
29. J.P. Burrows, A. Dehn, B. Deters, S. Himmelmann, A. Richter, S. Voigt, J. Orphal, J. Quantum Spectrosc. Radiat. Transf. **60**, 1025 (1998)
30. G.D. Greenblatt, J.J. Orlando, J.B. Burkholder, A.R. Ravishankara, J. Geophys. Res. **95**, 18577 (1990)
31. M. Mazurenka, R. Wada, A.J.L. Shillings, T.J.A. Butler, J.M. Beames, A.J. Orr-Ewing, Appl. Phys. B **81**, 135 (2005)
32. J.P. Burrows, A. Dehn, B. Deters, S. Himmelmann, A. Richter, S. Voigt, J. Orphal, J. Quantum Spectrosc. Radiat. Transf. **61**, 509 (1999)
33. R.J. Yokelson, J.B. Burkholder, R.W. Fox, R.K. Talukdar, A.R. Ravishankara, J. Phys. Chem. **98**, 13144 (1994)
34. L.S. Rothman, A. Barbe, D.C. Benner, L.R. Brown, C. Camy-Peyret, M.R. Carleer, K. Chance, C. Clerbaux, V. Dana, V.M. Devi, A. Fayt, J.-M. Flaud, R.R. Gamache, A. Goldman, D. Jacquemart, K.W. Jucks, W.J. Lafferty, J.-Y. Mandin, S.T. Massie, V. Nemtchinov, D.A. Newnham, A. Perrin, C.P. Rinsland, J. Schroeder, K.M. Smith, M.A.H. Smith, K. Tang, R.A. Toth, J. Vander Auwera, P. Varanasi, K. Yoshino, J. Quantum Spectrosc. Radiat. Transf. **82**, 5 (2003)
35. S.M. Ball, R.L. Jones, Chem. Rev. **103**, 5239 (2003)
36. T. Wagner, C. von Friedeburg, M. Wenig, C. Otten, U. Platt, J. Geophys. Res. **107**, 4424 (2002)
37. F. Wittrock, H. Oetjen, A. Richter, S. Fietkau, T. Medeke, A. Rozanov, J.P. Burrows, Atmos. Chem. Phys. **4**, 955 (2004)
38. U. Friess, P.S. Monks, J.J. Remedios, A. Rozanov, R. Sinreich, T. Wagner, U. Platt, J. Geophys. Res. **111**, D14203 (2006)